Recycling spent lithium-ion batteries using waste benzene-containing plastics: synergetic thermal reduction and benzene decomposition

*Baolong Qiu[a], Mengjie Liu[b], Xin Qu[c], Beilei Zhang[a], Hongwei Xie[a], Dihua Wang[c], Lawrence Yoon Suk Lee[b], Huayi Yin[a,c,d]**

a. Key Laboratory for Ecological Metallurgy of Multimetallic Mineral of Ministry of Education, School of Metallurgy, Northeastern University, Shenyang, 110819, P. R. China.

b. Department of Applied Biology and Chemical Technology and the State Key Laboratory of Chemical Biology and Drug Discovery, The Hong Kong Polytechnic University, Hung Hom, Kowloon, Hong Kong SAR, China.

c. School of Resource and Environmental Science, Wuhan University, Wuhan, 430072, P. R. China.

d. Key Laboratory of Data Analytics and Optimization for Smart Industry, Ministry of Education, Northeastern University, Shenyang, 110819, P. R. China.

Corresponding author: Huayi Yin yinhuayi@whu.edu.cn

Abstract: Spent lithium-ion batteries (LIBs) and benzene-containing polymers (BCPs) are two major pollutants that cause serious environmental burdens. Herein, spent LIBs and BCPs are co-pyrolyzed in a sealed reactor to generate Li_2CO_3, metals, and/or metal oxides without emitting toxic benzene-based gases. The use of a closed reactor allows the sufficient reduction reaction between the BCP-derived polycyclic aromatic hydrocarbon (PAH) gases and lithium transition metal oxides (LTMOs), achieving the Li recovery rates of 98.3, 99.9, and 97.5 % for $LiCoO_2$, $LiMn_2O_4$, and $LiNi_{0.6}Co_{0.2}Mn_{0.2}O_2$, respectively. More importantly, the thermal decomposition of PAHs (*e.g.*, phenol and benzene) is further catalyzed by the *in situ* generated Co, Ni, and MnO_2 particles, which form metal/carbon composites, and thus prevent the emissions of toxic gases. Overall, the co-pyrolysis in a closed system paves a green way to synergistically recycle spent LIBs and handle waste BCPs.

Synopsis: Synergistic pyrolysis of spent lithium-ion batteries and benzene-containing plastics achieves key metal extraction and toxic benzene-containing gas degradation.

Keywords: Spent lithium-ion batteries, waste plastics, pyrolysis reduction, Li recovery, polycyclic aromatic hydrocarbons degradation

TOC Art:

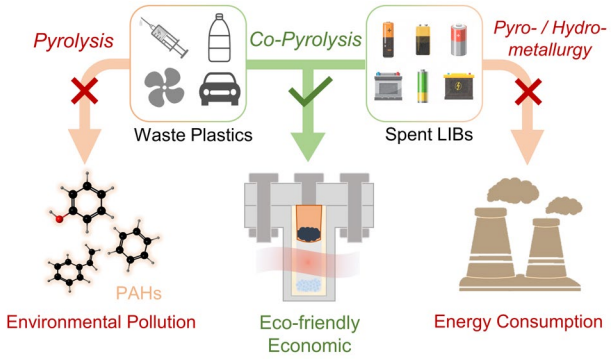

1. Introduction

Lithium-ion batteries (LIBs) and plastics play an important role in the modernization of our society and industries. The global production of LIBs is predicted to exceed 1.3 TWh by 2030,[1, 2] while the global plastic demand is projected to nearly triple to 1,100 million tons per year by 2050.[3] Despite the enormous conveniences brought to our society, spent LIBs and waste plastics also cause great harm to the environment.[4, 5] The large-scale production and consumption of LIBs demand a large and continuous supply of various natural resources.[2, 5, 6] According to the London Metal Exchange, the official price of Co reached US$ 72,500 per ton, and the average export price of Li_2CO_3 (battery grade, 99.5 %) increased to almost US$ 70,558 per ton in June of 2022.[7, 8] Spent LIB cathodes contain a large amount of Co and Li metal resources, however, the thermodynamic stability of lithium transition metal oxides (LTMOs) poses difficulties for recycling. For example, the separation of Li and transition metals needs strong mineral acids or high-temperature reduction processes with high energy consumption. In addition to spent LIBs, waste plastics are usually degraded into microplastics by photolysis and hydrolysis at a slow rate, which causes significant pollution in both water and land.[9, 10] In particular, the disposal of benzene-containing plastics (BCPs) in landfills can cause the immersion of harmful substances into groundwater and soil, while the incineration treatment generally releases toxic compounds such as dioxins and greenhouse gases into the atmosphere.[11, 12] For example, polycarbonate (PC) is a potential source of bisphenol A, which is an endocrine disruptor for human beings and animals.[13] A cost-effective and harmless approach to recycling and managing spent LIBs and plastic wastes are highly desired but very challenging to realize.

Pyrometallurgy is widely used in traditional recovery processes to recover critical metals from spent LIBs.[14-18] The pyrometallurgy needs reducing agents to reduce LTMOs by breaking the

chemical bonds between lithium and transition metals. Various reducing agents have been adopted to assist the reduction reaction, including carbon,[19] CO,[20] biomass,[21] corn stalk,[22] and polyvinyl chloride (PVC) plastics.[23] Carbothermic reduction is widely used to recover spent LIBs. However, it needs a higher temperature than other gaseous reductants such as CO and CH_4. Some organics that can form reducing gas upon pyrolysis have been also used as an alternative reducing agent. For instance, waste plastic is a promising reducing agent because of its abundant reserves but suffers from the difficulties of being reutilized.[24, 25] There are two challenges of using waste plastics as the reducing agent.[26, 27] First, the decomposition temperature of waste plastics is around 400 °C, at which the pyrolysis gases are not able to completely reduce LTMOs. Second, the pyrolysis of waste plastics generates toxic gases, which pose a threat to the environment. Especially, the decomposition of BCPs by thermochemical cracking produces polycyclic aromatic hydrocarbons (PAHs). For example, the pyrolytic decomposition of polycarbonate (PC), polystyrene (PS), polyethylene terephthalate (PET), and polybutylene terephthalate (PBT) produces gases containing phenol,[13,28] styrene,[29] and toluene.[30] These PAHs are typical carcinogens. Hence, a novel approach is required to enhance the reducing activity of organic gases without generating toxic gases for the development of pyrolysis reduction using waste BCPs.

Herein, we report the co-pyrolysis of spent LTMOs and BCPs in a gas-tight stainless-steel reactor (**Scheme 1**). The use of the gas-tight reactor keeps the pyrolysis gas in a closed space assuring the sufficient reduction of LTMOs and such *in situ* obtained transition metals can catalyze the decomposition of toxic PAHs. After pyrolysis, the Li_2CO_3 and transition metals can be obtained at the top of the reactor and separated by water leaching. The bottom product was hard carbon. We also systematically investigated the reduction process of three typical LTMOs ($LiCoO_2$

(LCO), $LiMn_2O_4$ (LMO), and $LiNi_{0.6}Co_{0.2}Mn_{0.2}O_2$ (NCM622)) using various BCPs (PC, PET, PBT, and PS).

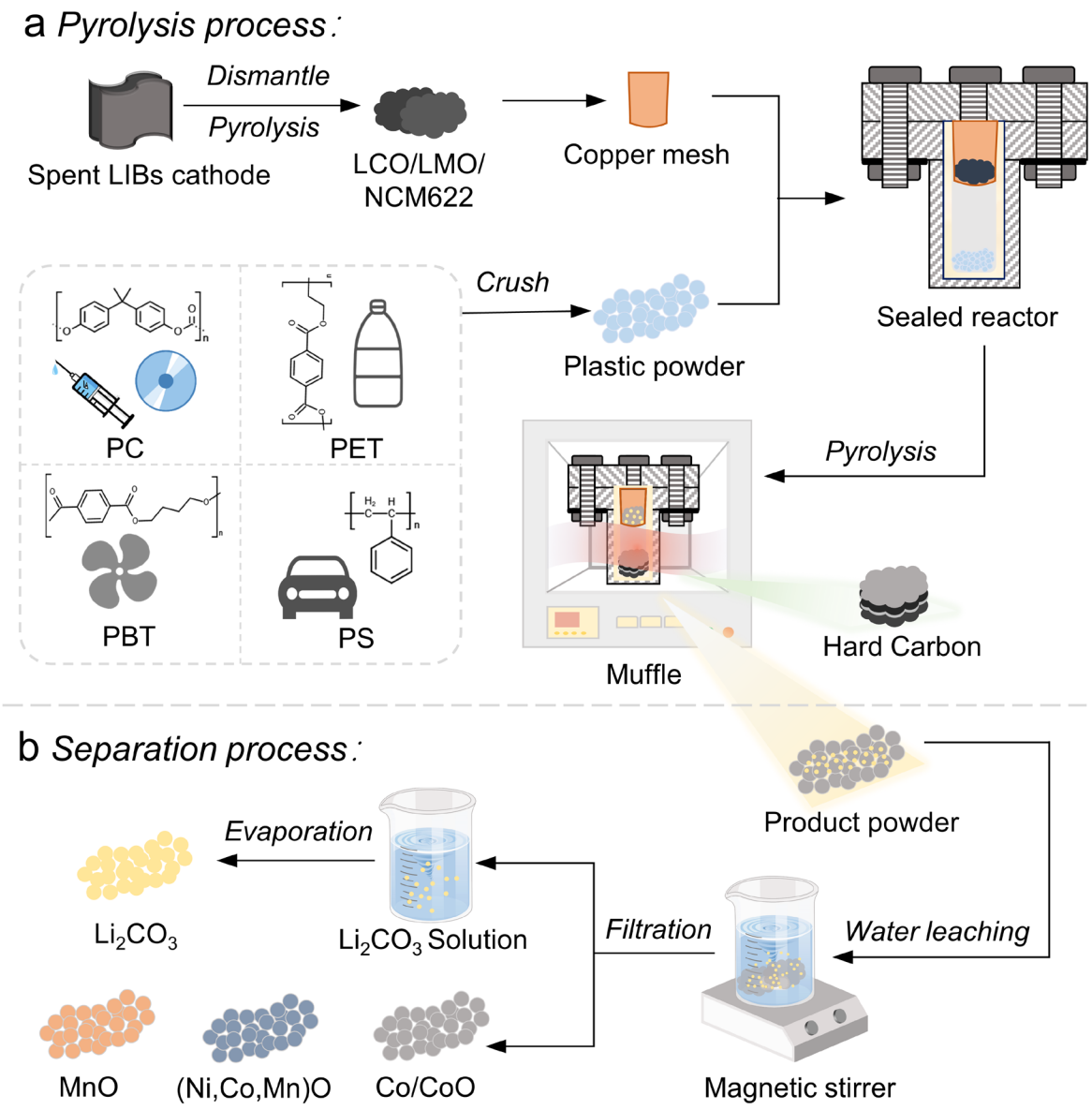

Scheme. 1. Schematic diagram of the recovery process of spent LIBs. (a) The dismantling of spent LIBs and pyrolysis processes, (b) Pyrolysis product separation.

2. Experimental Section

2.1 Chemicals and materials

Three commercial (AR grade) LTMO cathode materials, layered $LiCoO_2$ (LCO), spinel oxide $LiMn_2O_4$ (LMO), and layered $LiNi_{0.6}Co_{0.2}Mn_{0.2}O_2$ (NCM622) were purchased from Sinopharm Group Co. Ltd. Four types of plastic powders, polycarbonate (PC), polybutylene terephthalate (PBT), polyethylene terephthalate (PET), and polystyrene (PS) (>99.9 %), were obtained from Fengtai Polymer Materials Co. Ltd. All materials were used as received without further purification.

2.2 Experimental methods

The pyrolysis recovery experiment was carried out in a 50 mL sealed stainless-steel reactor using a muffle furnace. LCO was selected as the first example of pyrolysis reduction. LCO (0.5 g) contained in a copper mesh was suspended at the top of the reactor and PC (0.05 – 2 g) was put at the bottom of the reactor. The samples were heated to 400-550 °C (± 0.1 °C) for 30 to 300 min (ramping rate = 5 °C min^{-1}). After the reaction, the product in the copper mesh was poured into a 100 mL beaker containing 50 mL of ionized water, and the solution was stirred at 25 °C for 1 h. The solution was then poured into a funnel lined with a hydrophilic polyvinylidene hard pore membrane filter (90 mm in diameter, 0.45 μm in pore size), and the leachate was filtered into a 100 mL volume flask to obtain the filtrate and solid product. The metal ion concentration of the filtrate was measured and the leaching efficiency of metals (R_i) was calculated according to Equation (1). The as-obtained solid product was vacuum-dried at 60 °C for 24 h for further characterization. LMO and NCM622 were also used as the raw materials using the same method

for LCO, and PC, PET, PBT, and PS were used as the reducing agents to verify the viability of the reduction pyrolysis approach.

$$R_i(\%)=\frac{\text{moles of recovered element i}}{\text{moles of element in mixed powders}}\times 100\% \quad \text{(R-1)}$$

The contents of Li, Ni, Co, and Mn in the raw materials were determined by fully dissolving the cathode materials with aqua regia (a mixture of HCl and HNO_3, vol. ratio = 3:1) and measuring the element concentration using an atomic absorption spectrophotometer. All solutions were prepared with deionized water, and all chemical reagents used were analytical grade.

2.3 Economic and environmental analysis

The EverBatt model was used to perform the techno-economic and life-cycle analysis of three types of processes for recycling spent batteries: pyrometallurgy, hydrometallurgy, and direct cathode recycling.[31] It is a closed-loop battery recycling cost and environmental impacts model developed by Argonne National Laboratory.

2.4 Characterizations

The crystal phases and components of all pyrolysis products were measured using a Rigaku-T III X-ray diffractometer (XRD, equipped with Cu Kα radiation = 1.5406 Å, Shimadzu X-ray 6000) at a scan rate of 10° min^{-1} over a 2θ range from 10 to 90°. The concentrations of Li^+, Co^{2+}, Mn^{2+}, and Ni^{2+} in solutions were measured by an atomic absorption spectrophotometer (AAS, TAS-990). Thermogravimetry-differential scanning calorimeter (TG-DSC) was used to analyze the thermal process (NETZSCH STA 449F5). Thermogravimetry-Mass spectrometry (TG-MS) analysis was performed using a thermal analyzer (Thermo plus EV2/thermo mass photo) from 30 to 600 °C under an Ar atmosphere. Pyrolysis gases were analyzed by gas chromatography (GC, 9790H,

Zhejiang Fuli, Analytical Inc.). A scanning electron microscope (SEM, FEI Quanta FEG 250) was used to characterize the morphology and composition of materials. Raman spectra were recorded on a confocal micro-Raman spectroscopy system (Renishaw, inVia) with a 532 nm streamline laser excitation.

3. Results and discussion

3.1. Thermodynamic analysis

Thermodynamic calculations are performed to predict the possible reduction route of pyrolysis. Gibbs free energies are used to determine whether a reaction can proceed spontaneously and to compare which reaction is thermodynamically favorable. Generally, CO, H_2, and CH_4 are released during the early stage of pyrolysis of PC, and the PAHs with high boiling points are released as the pyrolysis temperature is increased.[13] Phenol is the main PAH product in this case. As shown in **Fig. 1a**, the degradation of phenol in a closed reaction system has two routes. In the first route (Route I), phenol reacts with LCO to produce Co and Li_2CO_3 while in the second one, phenol is further decomposed into H_2 on the surface of Co and simultaneously forms a carbon shell on Co. The second route (Route II) is similar to the preparation of carbon nanotubes by chemical vapor deposition (CVD).[32-36] In this case, the generated Co in Route I catalyzes the reaction in Route II. Therefore, LTMOs can be reduced and the decomposition of phenol can be simultaneously catalyzed during the pyrolysis reduction, preventing the release of toxic phenol.

During the pyrolysis, PC is decomposed into small organic compounds such as CO and phenol that can participate in the subsequent reaction as reducing agents. The condensation

deposition of organic molecules on Co and Ni can produce carbon species. Li *et al.* studied the specific mechanism of carbothermal reduction of $LiCoO_2$, and the main reaction mechanism of the pyrolysis process can be roughly divided into three stages.[37] First, LCO decomposes into CoO, O_2, and Li_2O. Second, graphite is partially oxidized to CO by O_2 released from LCO, and the CO greatly facilitates the thermal decomposition of LCO at high temperatures.[38-41] Third, the graphite and CO are oxidized by O_2 to generate CO_2, and Li_2O reacts with CO_2 to form Li_2CO_3. Finally, CoO is reduced to Co by graphite or CO. The pyrolysis mechanism of NCM622 is similar to that of LCO.[42] The reaction R-2 shows a thermal decomposition reaction of NCM622 to produce O_2 and metal oxides. When O_2 is consumed by the reducing agent, NCM622 continues to decompose. The reactions of metal oxides with CO and phenol are shown in R-3 to R-5 and R-6 to R-8, respectively. The reactions R-9 to R-11 represent the reduction of the metal oxides by the carbon layers on the surface.

(I) Pyrolysis of $Li(Ni_{0.6}Co_{0.2}Mn_{0.2})O_2$:

$$20Li(Ni_{0.6}Co_{0.2}Mn_{0.2})O_2 \rightarrow 10Li_2O + 12NiO + 4CoO + 4MnO_2 + 3O_2(g) \quad \text{(R-2)}$$

(II) Reduction of dissociation products:

(a) Thermal reduction of metal oxides by carbon monoxide:

$$CO(g) + CoO \rightarrow Co + CO_2(g) \quad \text{(R-3)}$$

$$CO(g) + NiO \rightarrow Ni + CO_2(g) \quad \text{(R-4)}$$

$$CO(g) + MnO_2 \rightarrow MnO + CO_2(g) \quad \text{(R-5)}$$

(b) Thermal reduction of metal oxides by phenol:

$$1/6C_6H_6O(g) + 1/3CoO \rightarrow 1/3Co + C + 1/2H_2O(g) \quad \text{(R-6)}$$

$$1/6C_6H_6O(g) + 1/3NiO \rightarrow 1/3Ni + C + 1/2H_2O(g) \quad \text{(R-7)}$$

$$1/6C_6H_6O(g) + 1/3MnO_2 \rightarrow 1/3MnO + C + 1/2H_2O(g) \quad \text{(R-8)}$$

(c) Carbothermic reduction:

$$C + 2CoO \rightarrow Co + CO_2(g) \quad \text{(R-9)}$$

$$C + 2NiO \rightarrow 2Ni + CO_2(g) \quad \text{(R-10)}$$

$$C + 2MnO_2 \rightarrow 2MnO + CO_2(g) \quad \text{(R-11)}$$

According to thermodynamic analysis (**Figs. 1b-c**), phenol is thermodynamically more reducible than CO, meaning that phenol is more reactive than CO. In other words, CoO, NiO, and MnO_2 will be preferentially reduced by phenol in an atmosphere containing both phenol and CO. Other pyrolysis gases such as CO, alcohols, alkenes, alkane, and benzenes are also generated and can be used as reducing agents to reduce LTMOs (**Supporting Information: Fig. S1**).[43-45] On the other hand, LTMOs act as an oxidant for decomposing these pyrolysis gases, especially PAHs. Thus, waste plastics can be used as raw materials to produce reducing gases to break the crystal structure of LTMOs to separate Li and transition metals, thereby avoiding the release of toxic gases.

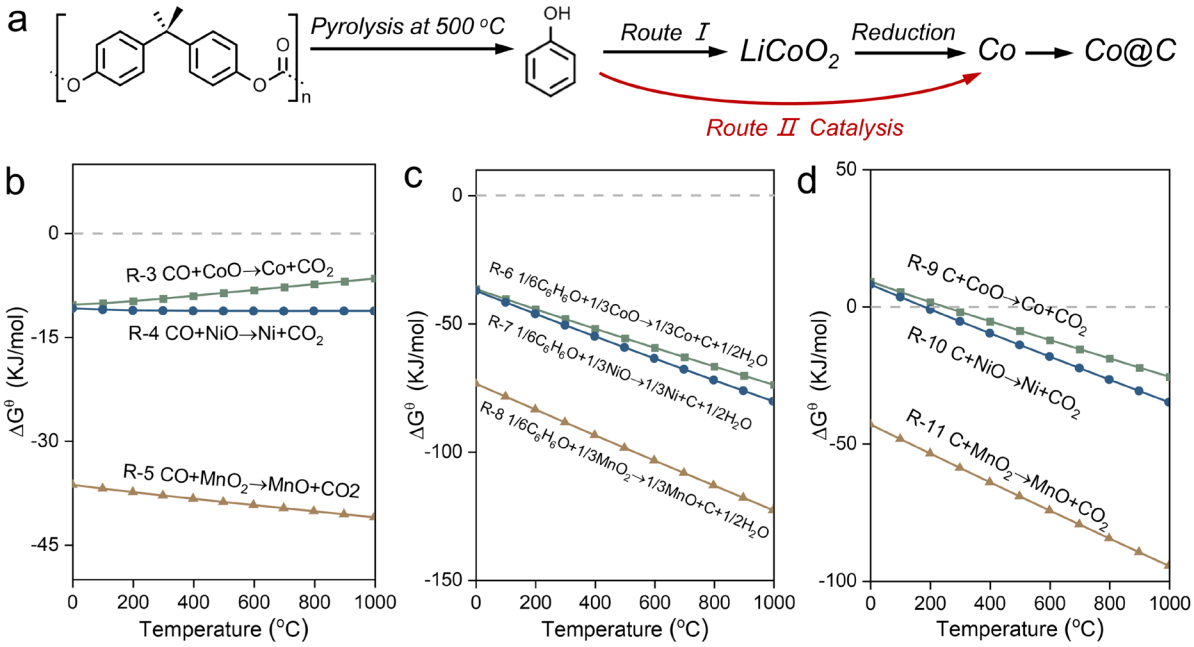

Fig. 1 (a) Two degradation routes of phenol. (b-d) Ellingham diagrams for possible reduction reactions: (b) reduction of metal oxides by CO, (c) reduction of metal oxides by phenol, and (d) carbothermal reduction. Thermodynamic analyses were carried out using HSC 9.0 with the activity values of all involved species set to unity (a = 1).

3.2. Thermal pyrolysis of BCPs and pyrolysis reduction

In situ TG-MS analysis was carried out to study the thermochemical degradation process of PC, PET, PBT, and PS under an Ar atmosphere. As shown in **Fig. 2a**, the onset decomposition temperatures for PC, PET, PBT, and PS are 501, 408, 435, and 410 °C, respectively. PC displays a mass loss of 77.0 % during the temperature change from 450 to 550 °C. The maximum mass loss rate of PET, PBT, and PS occurs at 434.9, 450.0, and 430.2 °C, respectively. The final masses of pyrolysis residues of PC, PET, PBT, and PS are 23.5, 12.9, 0.1, and 0.8 %, respectively. The gas generated from the PC pyrolysis contains CH_4 (6.3 %), CO (14.9 %), and phenol (0.9 %, **Fig. 2e**). The PET pyrolysis gases are CH_4 (3.2 %), C_2H_2 (0.9 %), CO (28 %), and toluene (1.8 %), while the PBT pyrolysis produces H_2 (1.7 %), HCN (4.4 %), CO (16.9 %), C_3H_4O (0.9 %), C_4H_6O (0.6 %), and C_6H_{12} (0.6 %). The PS pyrolysis gases consist of C_2H_2 (0.9 %), C_4H_2 (3.8 %), C_3H_5N (5.96 %), C_6H_6 (4.9 %), and C_8H_8 (3.8 %, **Figs. 2f-h**). Note that a large amount of styrene is formed during the pyrolysis of PS, which indicates that traditional incineration of PS is harmful to the environment. The detailed analyses of pyrolysis gas are given in **Supporting Information: Figs. S2-S9**. For comparison, pyrolysis gases produced in the presence of LCO were determined. At the temperature range between 300 and 500 °C, CH_4 is detected but disappears after the holding time of 1h, which suggests CH_4 participates in the pyrolysis reaction and is consumed as a reducing agent (**Supporting Information: Fig S10**). Other organic gases such as xxx and xxx are also consumed by pyrolysis reduction or catalytic decomposition, which demonstrates the advantage of toxic gas removal.

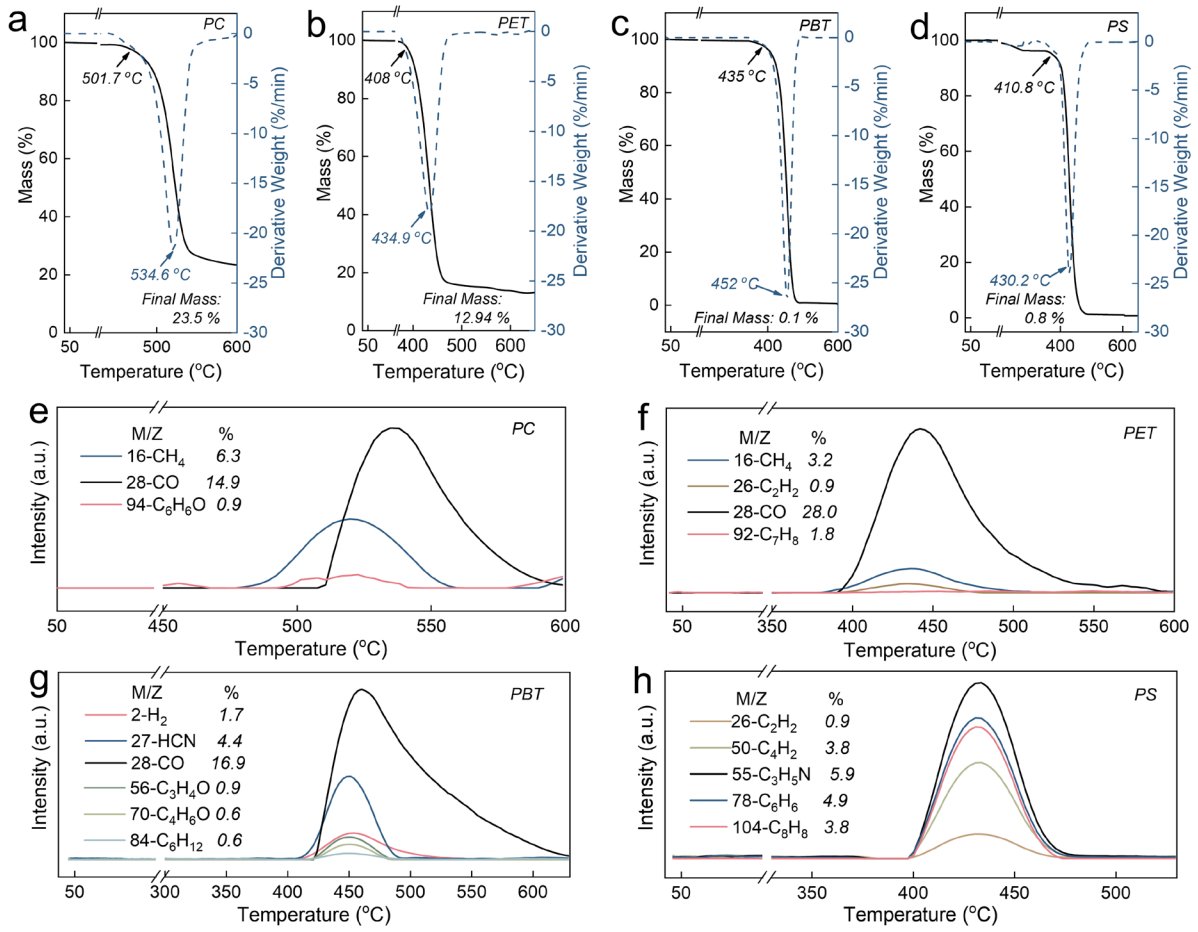

Fig. 2 TG curves of (a) PC, (b) PET, (c) PBT, and (d) PS. MS curves of (e) PC, (f) PET, (g) PBT, and (h) PS.

Based on thermodynamic and TG-MS analyses, 500 °C was chosen as the operating temperature because PC, PET, PBT, and PS decompose completely at this temperature. It should be pointed out that the closed stainless-steel reactor is necessary for capturing the pyrolysis gases and the increased pressure promotes the reduction of the spent cathode materials (**Supporting Information: Fig S11**). **Figs. 3a, 3c,** and **3e** show the XRD patterns of LCO, LMO, and NCM622 before and after pyrolysis reduction under different temperatures, respectively (LCO/PC mass ratio = 1:3, LMO/PC mass ratio = 1:0.1, NCM622/PC mass ratio = 1:3, reaction time = 5 h). At 400 °C, the diffraction peaks of LCO remain unchanged (**Fig. 3a**). As the temperature is raised to 450 °C,

the diffraction peaks of LCO disappear and the diffraction peaks of CoO appear. At 500 °C, the intensity of the CoO peak is dramatically weakened while the Co peak intensifies and a Li_2CO_3 peak appears. This suggests that the pyrolysis temperature affects the pyrolysis reduction because more pyrolysis gases are generated and their reduction kinetics is enhanced at a higher temperature. Similar phenomena are observed from the pyrolysis reduction of LMO and NCM622 (**Figs. 3c** and **3e**). When the temperature is raised from 400 to 500 °C, LMO is converted to MnO and Li_2CO_3, and NCM622 is reduced to Ni, Co, MnO, and Li_2CO_3. In addition to the pyrolysis temperature, the mass ratio of LTMO and PC also affects the reduction process because the amount of reducing gas and pressure are conducive to the complete reduction reaction (**Figs. 3b, 3d,** and **3f**). With the LCO/PC mass ratio of 1:0.05 (**Fig. 3b**), LCO is reduced to CoO. The CoO is further reduced to Co as the mass ratio is increased to 1:3, which indicates that the PC dosage is an important factor to limit the reduction reaction. In addition, LMO is reduced to MnO when the LMO/PC mass ratio is 1:0.1 (**Fig. 3d**). MnO can not be further reduced to Mn due to thermodynamic limitation but $MnCO_3$ is formed when it reacts with CO_2. As shown in **Fig. 3f**, the reduction products contain NiO, Ni_xMn_yO, and CoO when the NCM622/PC mass ratio is 1:0.1. With the increased mass ratio of 1:1, NiO and CoO are gradually reduced to Co and Ni. However, at the mass ratio of 1:3, NiO is completely reduced and $MnCO_3$ is generated. The XRD patterns of pyrolysis reduction products of LCO, LMO, and NCM622 under various holding times are shown in **Supporting Information** (**Figs S12-S14**). The pyrolysis gases can reduce LCO, LMO, and NCM622 to metals/metal oxides and Li_2CO_3 at a temperature below 550 °C.

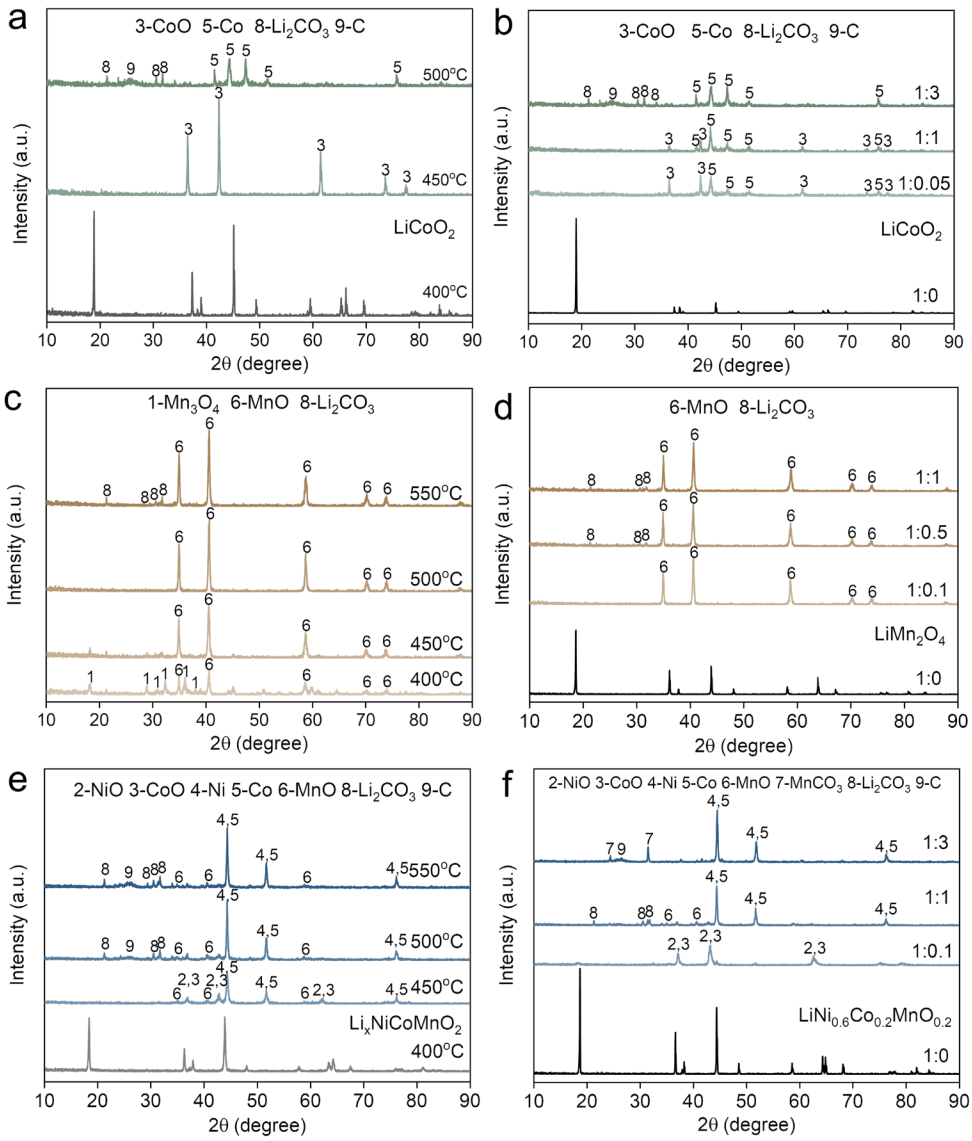

Fig. 3 XRD patterns of various cathode materials under different temperatures: (a) LCO (LCO/PC mass ratio = 1:3, 5 h), (c) LMO (LMO/PC mass ratio = 1:0.1, 5 h), (e) NCM622 (NCM622/PC mass ratio = 1:3, 5 h), and under different mass ratios: (b) LCO (500 °C, 5 h), (d) LMO (500 °C, 5 h), (f) NCM622 (500 °C, 5 h)

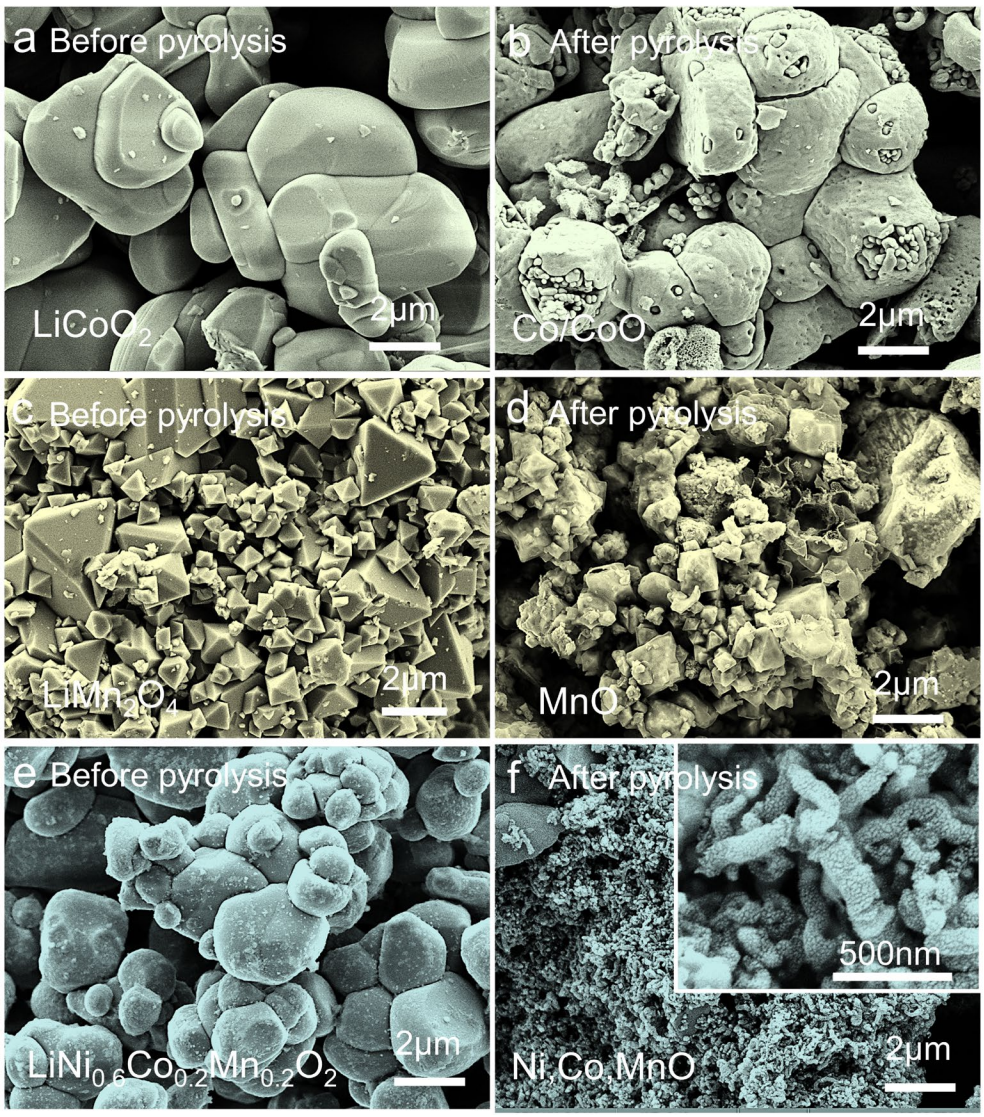

Fig. 4 SEM images of pristine (a) LCO, (c) LMO, and (e) NCM622. SEM images after pyrolysis reduction at 500 °C for 3 h: (b) LCO (LCO/PC mass ratio = 1:0.05), (d) LMO (LMO/PC mass ratio = 1:0.1), and (f) NCM622 (NCM622/PC mass ratio = 1:3).

The changes in the morphology of LCO, LMO, and NCM622 during the pyrolysis reduction are compared in **Fig. 4**. The pristine LCO particles of spherical shape have a diameter of roughly 10-20 μm with smooth surfaces (**Fig. 4a**). The microstructure of the cathode material is destroyed after pyrolysis reduction. As shown in **Fig. 4b**, a large number of defects is evident on the surface of the LCO, which is caused by the destruction of the crystal structure. When the LCO/PC mass

ratio of 1:3 (under 450 °C, 3 h) is used, core-shell structured CoO is observed (**Supporting Information: Figs S15-S17**). The pyrolysis at 500 °C reduces CoO to Co of nanoflower-like morphology (**Supporting Information: Fig S18**). Pristine LMO exhibits a typical spinel structure **(Fig. 4c**) that is well-retained after the reduction to MnO (**Fig. 4d**). NCM622 of similar morphology and size to LCO (**Fig. 4e**) is converted to nanorod-like structures by pyrolysis reduction (**Fig. 4f**). A large number of nanoparticles are distributed on the surface of carbon nanorods, whose large surface area is beneficial for the catalytic decomposition of BCPs. The changes in the mass ratio induce the morphology changes of pyrolysis products. When the mass ratio is increased from 1:1 to 1:2 (under 500 °C, 3 h), carbon nanotubes are grown on the surface of the nano-catalysts (**Supporting Information: Figs S20-S25**). In addition, the PC pyrolysis process also produces hard carbon on the bottom of the reactor (**Supporting Information: Fig S26**).

3.3. Recovery of Li, transition metals, and carbon

As shown in **Fig. 5a**, the leaching efficiency of Li is only 0.5 % at 400 °C, which indicates that almost no Li is released during the pyrolysis reduction of LCO. When the temperature reaches 500 °C, the leaching efficiency of Li increases to 98.3 % thanks to the promoted PC pyrolysis as well as the LCO reduction kinetics. The effect of the LCO/PC mass ratio on the leaching efficiency of Li was studied under different conditions. As shown in **Fig. 5b**, a low LCO/PC mass ratio promotes the reduction because more organic gases are produced. The duration of pyrolysis also affects the leaching efficiency of Li. As shown in **Fig. 5c**, the leaching efficiency of Li increases from 93.3 to 98.3 % when the holding time is extended from 30 to 180 min. This means that the pyrolysis reduction rate is fast under controlled temperatures and gas supply. Based on the above results, the optimal condition has been established as 500 °C, LCO/PC mass ratio of 1:3, and 3-h holding time.

In the water leaching process, the leaching efficiency of Co is less than 0.1 %. The standard solutions of four elements (Li^{+}, Co^{2+}, Mn^{2+}, and Ni^{2+}) were used to construct each calibration concentration curve (**Supporting Information: Fig S27**).

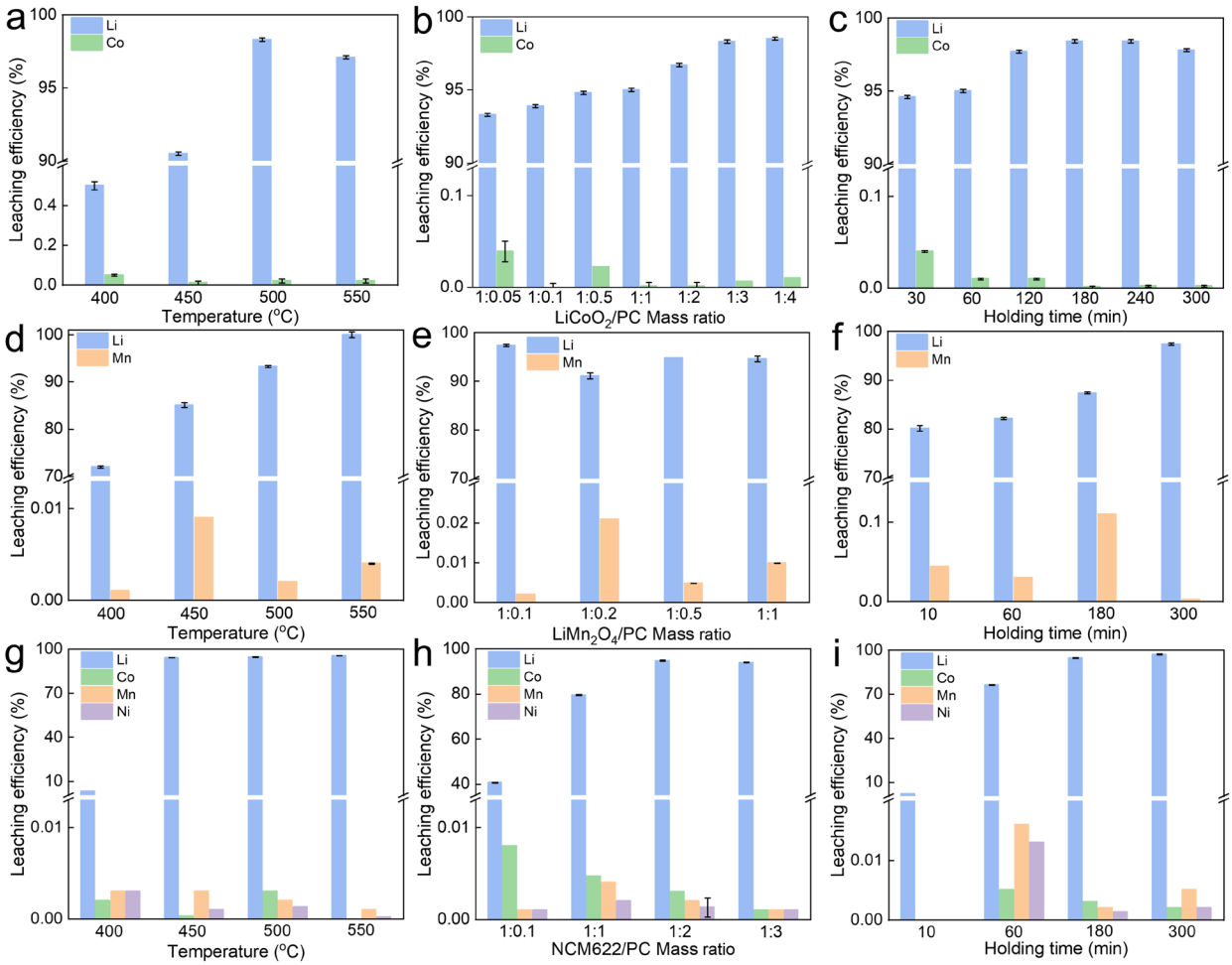

Fig. 5 Optimization of metal recovery from the pyrolysis reduction of LCO, LMO, and NCM622 with PC. (a) LCO (5 h, LCO/PC = 1:3), (b) LMO (5 h, LMO/PC = 1:0.1), (c) NCM622 (5 h, NCM/PC = 1:3) under different temperatures; (d) LCO (500 °C, 5h), (e) LMO (500 °C, 5 h), (h) NCM622 (500 °C, 5h) under different LTMO/PC mass ratios; and (c) LCO (500 °C, 1:3), (f) LMO (500 °C, 1:0.1), (i) NCM622 (500 °C, 1:3) under different holding times.

The leaching efficiency of Li in the pyrolysis reduction of LMO was studied under different mass ratios (500 °C, 5 h). As shown in **Fig. 5d**, the leaching efficiencies of Li are 72.0 % (400 °C),

85.1 % (450 °C), 93.9 % (500 °C), and 99.9 % (550 °C). The effect of the LMO/PC mass ratio on Li leaching efficiency was also investigated. As shown in **Fig. 5e**, the leaching efficiency of Li reaches 97.4 % when the LMO/PC mass ratio is 1:0.1. Compared with LCO, LMO is easier to be reduced because the consumption of PC is less than that of LCO. However, when the LMO/PC mass ratio is 1:1, the leaching efficiency of Li decreases to 94.6 % because MnO cannot catalyze PAHs. These undegraded PAHs condense to form oils that do not participate in the pyrolysis reduction. In addition, these oils coat Li_2CO_3 and prevent the leaching of Li. After 5 h (500 °C, LMO/PC mass ratio of 1:0.1), the Li leaching efficiency reaches 97.4 % (**Fig. 5f**). So, the optimal reduction conditions of recovering LMO are set as 550 °C with an LMO/PC mass ratio of 1:0.1 for a holding time of 5 h. After water leaching, the Mn leaching efficiency is less than 0.1 %.

The effects of pyrolysis reduction parameters on recovering NCM622 are summarized in **Figs. 5g–i**. The Li-leaching efficiency rises from 3.2 to 94.4 % with the increase of temperature from 400 to 450 °C (**Fig. 5g**), while it increases from 40.7 to 94 % as the NCM622/PC mass ratio is decreased from 1:0.1 to 1:3 (**Fig. 5h**). The leaching efficiency of Li reaches the highest value of 97.3 % with the reacting time extended to 5 h (**Fig. 5i**). The optimal pyrolysis conditions for NCM622 recovery are, thus, selected as 500 °C, 1:3 NCM622/PC mass ratio, and 5 h reaction time. The pyrolysis products of NCM622 using PC show very low (< 0.02 %) leaching efficiencies for Co, Ni, and Mn, which can be crystallized to form high-purity Li_2CO_3 by evaporation (**Supporting Information: Fig S28**).

3.4 Pyrolysis reduction with PBT, PET, and PS

The pyrolysis products of different plastics (PBT, PET, and PS) with LCO (at 500 °C, 3 h, LCO/plastic mass ratio of 1:3) were studied. As shown in **Fig. 6a**, LCO is reduced to Co and/or CoO, which indicates that the pyrolysis gases of these plastics can react with LCO. The

decomposition temperature is 250-350 °C for PET and PBT while 300-400 °C is needed for PS. A lower thermal decomposition temperature increases the yield of reducing gases, which would change the pyrolysis reduction process. In addition, PET and PBT produce benzene macromolecular organic compounds,[46-48] and PS produces styrene.[49, 50] LMO is reduced to MnO and generates Li_2CO_3 when PC, PBT, and PET are used as pyrolysis agents (**Fig. 6c**). However, the reduction of LMO to MnO is incomplete when PS is used. Such incomplete reduction is maybe because the PS pyrolysis produces fewer reduction gases and the MnO has no catalytic ability to decompose PAHs to small reducing molecules such as H_2 and CO. Thus, the produced metal oxides or metals are important in catalyzing the decomposition of PAHs to generate more reducing gases that help reduce the LTMOs. The products of NCM622 are Ni, Co, and MnO (**Fig. 6e**).

As shown in **Fig. 6b**, the leaching efficiencies of Li are 98.3 % for PC, 94.3 % for PBT, 92.9 % for PET, and 81.5 % for PS with the conditions of LCO/plastic mass ratio of 1:3 at 500 °C for 3 h. When the plastics are pyrolyzed with an LMO/plastic mass ratio of 1:0.1 at 500 °C for 5 h, the Li leaching efficiencies are 99.98 % for PC, 97.51 % for PBT, 94.95 % for PET and 63.58 % for PS (**Fig. 6d**). In addition, the leaching efficiencies of Li are 97.25 % for PC, 95.51 % for PBT, 95.95 % for PET and 73.58 % for PS when the plastics are pyrolyzed with an NCM622/plastic mass ratio of 1:3 at 500 °C for 5 h (**Fig. 6f**). The relatively low Li leaching efficiencies when PS is used as the reducing agent in all three LTMOs may be due to the large amount of macromolecular gas produced by PS, which cannot decompose and reduce the LTMOs. Therefore, the component of the pyrolysis gas is another important factor governing the pyrolysis reduction. The co-pyrolysis results of spent LCO and NCM622 with waste PET plastic are consistent with the model (**Supporting Information: Fig S29**)

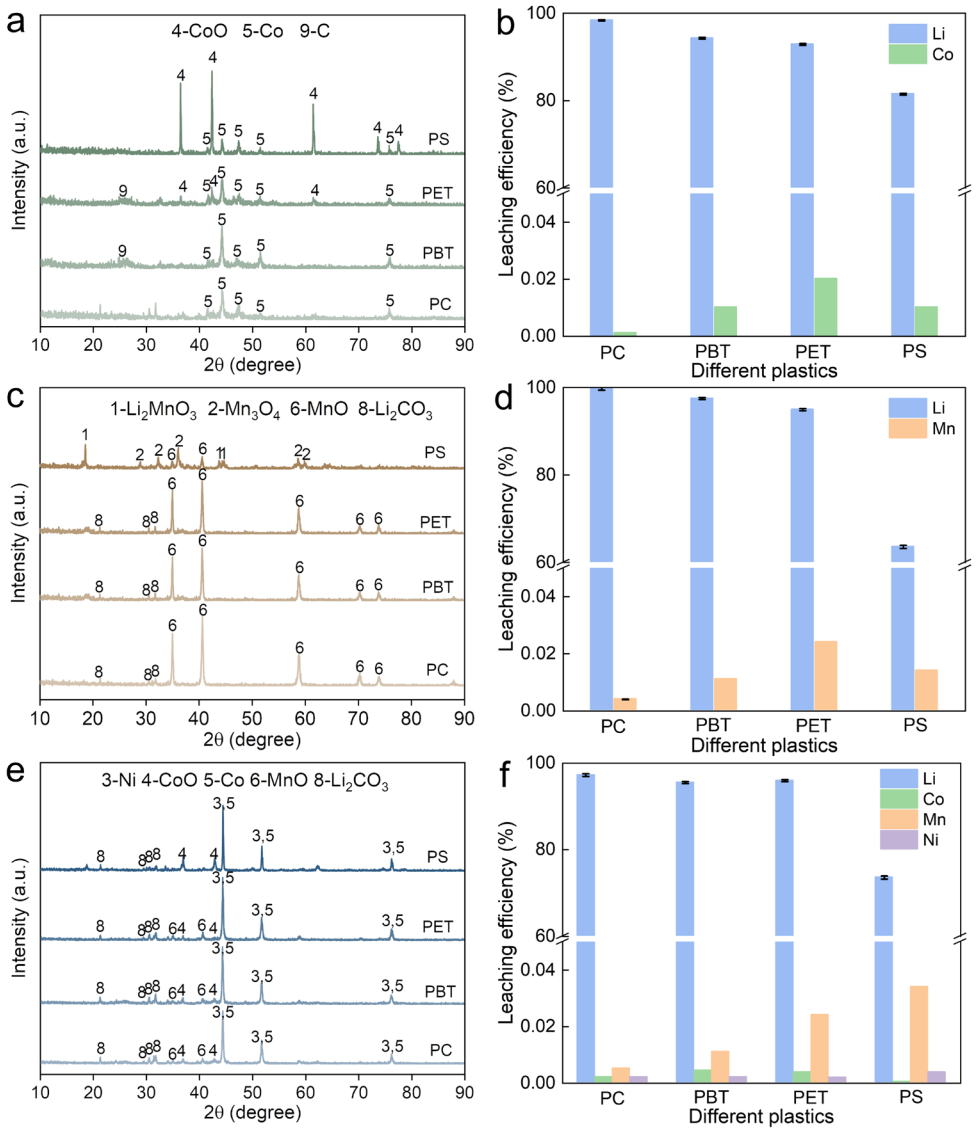

Fig. 6 XRD patterns of different plastics (PBT, PET, PS) pyrolyzed with (a) LCO (500 °C, 3 h, LCO/selected plastic mass ratio of 1:3), (c) LMO (550 °C, 5 h, LMO/selected plastic mass ratio of 1:0.1), (e) NCM622 (500 °C, 5 h, NCM622/selected plastic mass ratio of 1:3), the leaching efficiency of Li, Co, Mn, Ni (b) LCO, (d) LMO, (f) NCM622.

3.5 TG-DSC analysis with *in situ* pyrolysis process and mechanism

The thermal processes of the mixture of PC and LCO or NCM622 were performed to study the pyrolysis reduction process. The thermogravimetry/differential scanning calorimetry (TG-DSC)

curves of both LCO-PC (**Fig. 7a**) and NCM622-PC mixtures (**Fig. 7b**) show a similar trend in the temperature range of 30-600 °C. The pyrolysis process can be divided into two stages. In the first stage from 350 to 450 °C, significant mass losses of 48.8 and 45.2 % are observed from LCO-PC and NCM622-PC, respectively, which may be caused by the reaction of small organic molecules produced by PC with cathode materials. In the second stage from 450 to 600 °C, the mass losses of 5.7 and 6.8 % indicate that the reaction between the PC-derived gas and cathode material is mostly completed and the PC continues to decompose with the increase in temperature. The DSC curves show two exothermic processes in the pyrolysis of the LCO-PC system (384.6 and 487.2 °C) and NCM622-PC system (369.1 and 486.2 °C). These two processes correspond to the decomposition of PC and the pyrolysis reduction of the LCO and NCM622.

The reaction process was visualized using advanced temperature/pressure monitoring equipment (**Supporting Information: Fig S30**). As shown in **Fig. 7c**, the temperature and pressure vary with the pyrolysis time. According to the pressure change, the reaction can be divided into three steps. The first step is the pyrolysis of plastic, which occurs at a temperature between 400.3 and 498.4 °C under the pressure range from 0.1 to 0.46 MPa. The second step is the pyrolysis reduction reaction. The pressure reaches a plateau and stabilizes at about 0.46-0.49 MPa at 500 °C. This state is maintained for 64 min, reducing NCM622 to Co and Ni. The third step is the catalysis process. The internal pressure of the reactor begins to rise from 0.49 to 0.80 MPa when the holding time is increased from 164 to 440 min, indicating that PAHs are dehydrogenated to produce hydrogen.

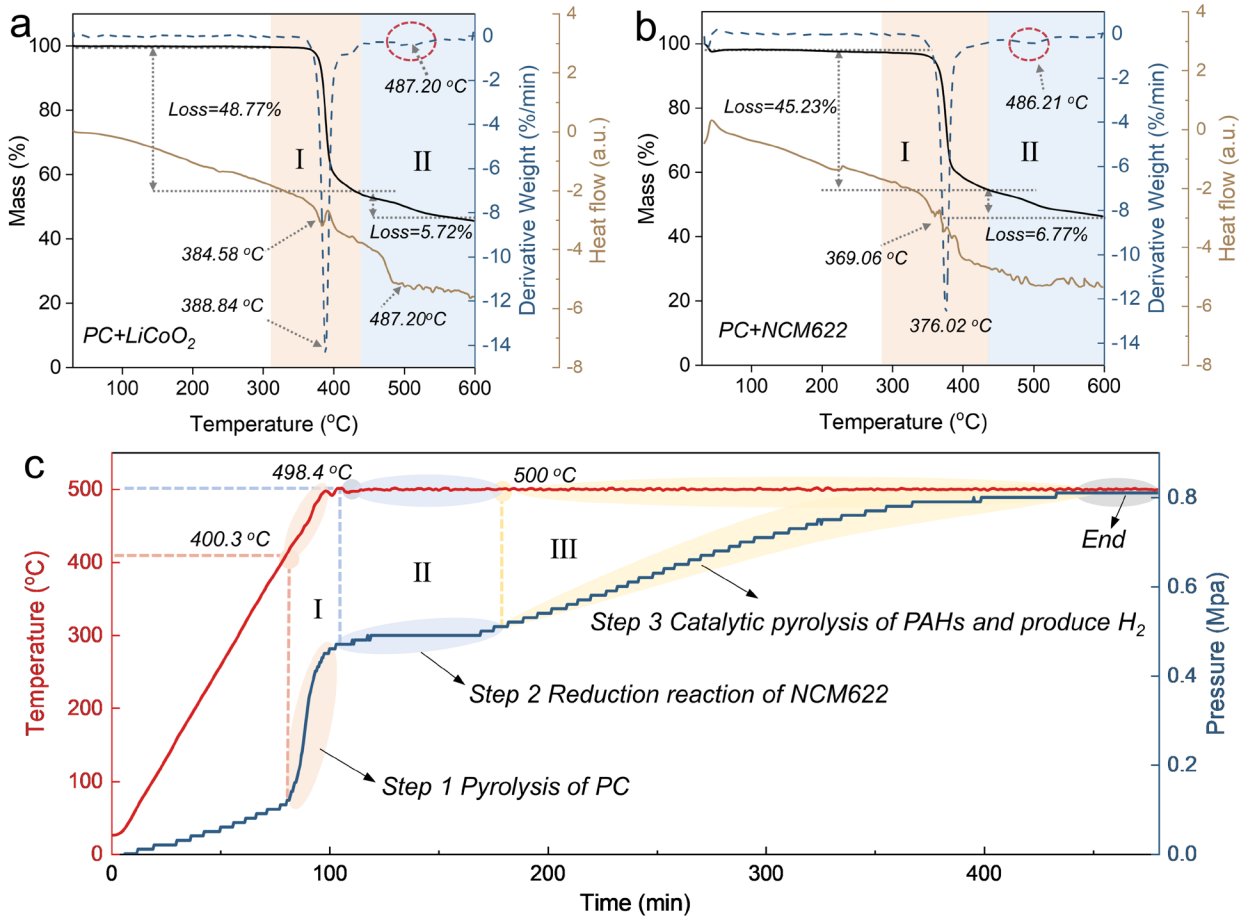

Fig. 7 TG-DSC curve of the pyrolysis reduction of (a) LCO with PCs, and (b) NCM622 with PC. (c) Temperature and gas pressure profiles of the pyrolysis reduction of the NCM622 and PC mixture as a function of time (NCM622/PC mass ratio = 1:1).

The proposed mechanism of the pyrolysis reduction of LCO-PC is illustrated in **Scheme 2**. First, PC is decomposed to generate organic gases such as CH_4, CO, and PAHs when the temperature reaches above the decomposition temperature of plastics. Second, the generated organic gases react with LCO to generate CoO and/or Co and liberate Li_2O gradually. At the same time, Li_2O reacts with CO_2 to form Li_2CO_3. Finally, the dehydrogenation reaction of PAHs (*e.g.*, phenol and benzene) is catalyzed by Co, resulting in the generation of H_2, CO, and carbon. The PAHs-derived gases continue to participate in the reduction of LCO or CO. Therefore, the co-

pyrolysis achieves the goal of using reducing gases as well as preventing the generation of toxic gases.

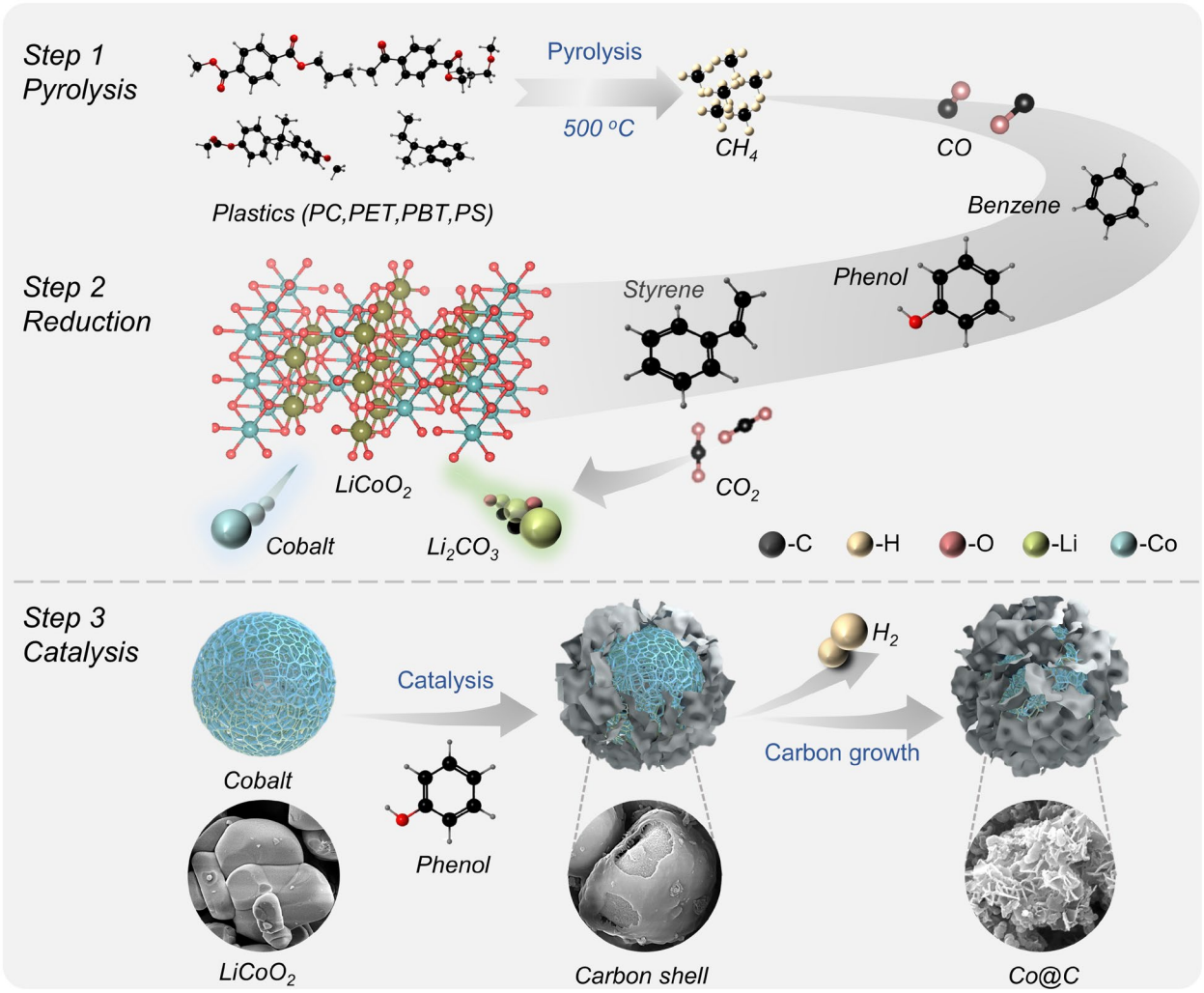

Scheme. 2 The mechanism of LCO with PC pyrolysis process.

3.6 Economic and environmental analysis

The economic impact of the reduction recovery process of BCPs was evaluated using the EverBatt model[31] and compared with commercial pyrometallurgical and hydrometallurgical recovery processes.[51] It should be noted that energy consumption and greenhouse gas (GHG) emissions and

revenues are based on hydrometallurgy, which is currently the most widely used method in the spent battery recycling industry. The details of the evaluation process using the EverBatt model can be found in the **Supporting Information: Figs S31-36**.

Assuming an annual processing capacity of 10,000 tons of spent LIBs at a U.S. plant, three different recycling methods are modeled. As shown in **Fig. 8a**, the total life cycle energy consumption of the pyrometallurgical and hydrometallurgical processes are 12.06 and 20.01 MJ kg^{-1} LCO batteries, respectively. Hydrometallurgy is expected to have the highest energy consumption (90 %), mainly due to a large amount of material input from upstream production. In the pyrometallurgy process, 33 % of energy consumption is attributed to high-temperature smelting. The total energy consumption of BCPs recovery is only 10.01 MJ kg^{-1} LCO battery, which is only 50 % of that of hydrometallurgy. GHG emission is also an important factor to consider when evaluating recovery methods. As shown in **Fig. 8b**, pyrometallurgical GHG emissions mainly come from process emissions (smelting), while hydrometallurgical GHG emissions mainly come from the contribution of upstream chemicals. It should be noted that the total GHG emissions released by the recycling of BCPs are only 44 % of the emissions from hydrometallurgy. The direct regeneration process is expected to generate the highest revenue (**Fig. 8c**) because the recovered cathode product can be directly used to produce new LCO cathode, which is of higher value than the precursors produced in pyrometallurgy and hydrometallurgy.

The spider chart shown in **Fig. 8d** comprehensively compares three recycling methods. In terms of energy efficiency, low emission, and revenue, the plastic pyrolysis reduction and recovery process are superior to pyrometallurgy and hydrometallurgy because the pyrolysis reaction happens at 400-500 °C and does not use a lot of chemical reagents. By comparing the processes of pyrometallurgy and hydrometallurgy, the pyrolysis process of plastic as a reducing agent is

simple and safe. Note that the calculation is only used for estimation because this process is only tested on a lab scale, and it could be different when the process is scaled up for industrial application. In addition, the value of the carbon is not included in the current calculation. Thus, the revenue may be higher if the value of carbon is considered.

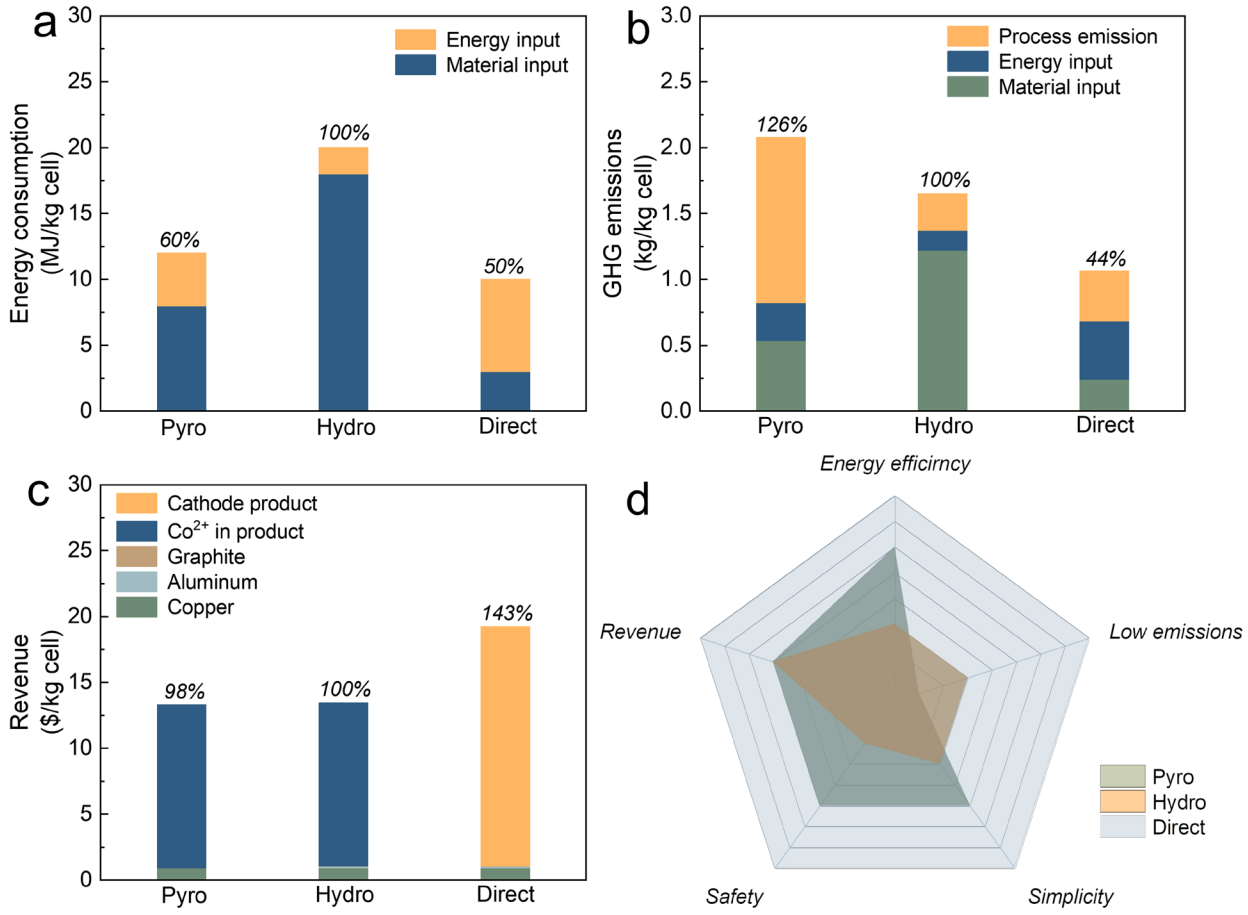

Fig. 8 Economic and environmental analysis of pyrometallurgical (Pyro), hydrometallurgical (Hydro), and plastics reduction (Direct) recycling methods. (a) Energy consumption, (b) GHG emissions, (c) potential revenue from outputs produced, (d) a spider chart comparing various features of Pyro, Hydro, and Direct recycling methods.

Author Information:

Corresponding Author

Huayi Yin: Key Laboratory for Ecological Metallurgy of Multimetallic Mineral of Ministry of Education, School of Metallurgy, Northeastern University, Shenyang, 110819, P. R. China. School of Resource and Environmental Science, Wuhan University, Wuhan, 430072, P. R. China. Key Laboratory of Data Analytics and Optimization for Smart Industry, Ministry of Education, Northeastern University, Shenyang, 110819, P. R. China; Email: yinhuayi@whu.edu.cn

Authors

Baolong Qiu: Key Laboratory for Ecological Metallurgy of Multimetallic Mineral of Ministry of Education, School of Metallurgy, Northeastern University, Shenyang, 110819, P. R. China.

Mengjie Liu: Department of Applied Biology and Chemical Technology and the State Key Laboratory of Chemical Biology and Drug Discovery, The Hong Kong Polytechnic University, Hung Hom, Kowloon, Hong Kong SAR, P. R. China.

Xin Qu: School of Resource and Environmental Science, Wuhan University, Wuhan, 430072, P. R. China.

Beilei Zhang: Key Laboratory for Ecological Metallurgy of Multimetallic Mineral of Ministry of Education, School of Metallurgy, Northeastern University, Shenyang, 110819, P. R. China.

Hongwei Xie: Key Laboratory for Ecological Metallurgy of Multimetallic Mineral of Ministry of Education, School of Metallurgy, Northeastern University, Shenyang, 110819, P. R. China.

Dihua Wang: School of Resource and Environmental Science, Wuhan University, Wuhan, 430072, P. R. China.

Lawrence Yoon Suk Lee: Department of Applied Biology and Chemical Technology and the Research Institute for Smart Energy, The Hong Kong Polytechnic University, Hung Hom, Kowloon, Hong Kong SAR, P. R. China.

Supporting Information

Ellingham diagrams for possible reduction reactions. Fraction concentration and hotspot of plastics pyrolysis gas. Standard concentration curve. GC-MS of four plastics. XRD, TEM, and Raman patterns of products under different pyrolysis conditions. Economic and environmental evaluation of the EverBatt model.

Acknowledgments:

We greatly thank the financial support from the Fundamental Research Funds for the Central Universities (N2025034, N2025035), Xingliao Project (XLYC 1807042), and the 111 Project (B16009).

References

1. Zheng, M.; Salim, H.; Liu, T.; Stewart, R. A.; Lu, J.; Zhang, S., Intelligence-assisted predesign for the sustainable recycling of lithium-ion batteries and beyond. *Energy Environ. Sci.* **2021,** *14* (11), 5801-5815.

2. Ziegler, M. S.; Song, J.; Trancik, J. E., Determinants of lithium-ion battery technology cost decline. *Energy Environ. Sci.* **2021,** *14* (12), 6074-6098.

3. Zibunas, C., Meys, R., Kätelhön, A., & Bardow, A. (2022). Cost-optimal pathways towards net-zero chemicals and plastics based on a circular carbon economy. *Comput. Chem. Eng. 2022*, 162, 107798-.

4.Harper, G.; Sommerville, R.; Kendrick, E.; Driscoll, L.; Slater, P.; Stolkin, R.; Walton, A.; Christensen, P.; Heidrich, O.; Lambert, S.; Abbott, A.; Ryder, K.; Gaines, L.; Anderson, P., Recycling lithium-ion batteries from electric vehicles. *Nature* **2019,** *575* (7781), 75-86.

5.Chen, M.; Ma, X.; Chen, B.; Arsenault, R.; Karlson, P.; Simon, N.; Wang, Y., Recycling end-of-life electric vehicle lithium-Ion batteries. *Joule* **2019,** *3* (11), 2622-2646.

6.Ma, X.; Chen, M.; Zheng, Z.; Bullen, D.; Wang, J.; Harrison, C.; Gratz, E.; Lin, Y.; Yang, Z.; Zhang, Y.; Wang, F.; Robertson, D.; Son, S.-B.; Bloom, I.; Wen, J.; Ge, M.; Xiao, X.; Lee, W.-K.; Tang, M.; Wang, Q.; Fu, J.; Zhang, Y.; Sousa, B. C.; Arsenault, R.; Karlson, P.; Simon, N.; Wang, Y., Recycled cathode materials enabled superior performance for lithium-ion batteries. *Joule* **2021,** *5* (11), 2955-2970.

7.L.M.T Cobalt. https://www.lme.com/en/Metals/EV/LME-Cobalt#Trading+day+summary.

8.S.M.M Lithium Carbonate. https://www.metal.com/Chemical-Compound/201905160001.

9.Mitrano, D. M.; Wick, P.; Nowack, B., Placing nanoplastics in the context of global plastic pollution. *Nat Nanotechnol* **2021,** *16* (5), 491-500.

10.Song, X.; Lyu, M.; Zhang, X.; Ruthensteiner, B.; Ahn, I.-Y.; Pastorino, G.; Wang, Y.; Gu, Y.; Ta, K.; Sun, J.; Liu, X.; Han, J.; Ke, C.; Peng, X., Large plastic debris dumps: new biodiversity hot spots emerging on the deep-sea floor. *Environ. Sci. Technol. Lett.* **2021,** *8* (2), 148-154.

11.Chu, S.; Zhang, B.; Zhao, X.; Soo, H. S.; Wang, F.; Xiao, R.; Zhang, H., Photocatalytic conversion of plastic waste: from photodegradation to photosynthesis. *Adv. Energy Mater.* **2022,** *12* (22).

12.Anuar Sharuddin, S. D.; Abnisa, F.; Wan Daud, W. M. A.; Aroua, M. K., A review on pyrolysis of plastic wastes. *Energy Convers. Manage.* **2016,** *115*, 308-326.

13.Lee, T.; Jung, S.; Baek, K.; Tsang, Y. F.; Lin, K. A.; Jeon, Y. J.; Kwon, E. E., Functional use of CO2 to mitigate the formation of bisphenol A in catalytic pyrolysis of polycarbonate. *J. Hazard Mater* **2022,** *423* (Pt A), 126992.

14.Ordoñez, J.; Gago, E. J.; Girard, A., Processes and technologies for the recycling and recovery of spent lithium-ion batteries. *Renewable Sustainable Energy Rev.* **2016,** *60*, 195-205.

15.Fan, E.; Li, L.; Wang, Z.; Lin, J.; Huang, Y.; Yao, Y.; Chen, R.; Wu, F., Sustainable recycling technology for Li-Ion batteries and beyond: challenges and future prospects. *Chem. Rev.* **2020,** *120* (14), 7020-7063.

16. Fang, J., Ding, Z., Ling, Y., Li, J., Zhuge, X., Luo, Z., Ren, Y., & Luo, K. (2022). Green recycling and regeneration of LiNi0.5Co0.2Mn0.3O2 from spent Lithium-ion batteries assisted by sodium sulfate electrolysis. *Chem. Eng. J.* (Lausanne, Switzerland : 1996), **2022,** 440, 135880.

17.Fan, M.; Chang, X.; Guo, Y.-J.; Chen, W.-P.; Yin, Y.-X.; Yang, X.; Meng, Q.; Wan, L.-J.; Guo, Y.-G., Increased residual lithium compounds guided design for green recycling of spent lithium-ion cathodes. *Energy Environ. Sci.* **2021,** *14* (3), 1461-1468.

18.Xiao, J.; Li, J.; Xu, Z., Novel approach for in situ recovery of lithium carbonate from spent lithium Ion batteries using vacuum metallurgy. *Environ. Sci. Technol.* **2017,** *51* (20), 11960-11966.

19.Xu, P.; Liu, C.; Zhang, X.; Zheng, X.; Lv, W.; Rao, F.; Yao, P.; Wang, J.; Sun, Z., Synergic mechanisms on carbon and sulfur during the selective recovery of valuable metals from spent lithium-Ion batteries. *ACS Sustain. Chem. Eng.* **2021,** *9* (5), 2271-2279.

20.Peng, Q.; Zhu, X.; Li, J.; Liao, Q.; Lai, Y.; Zhang, L.; Fu, Q.; Zhu, X., A novel method for carbon removal and valuable metal recovery by incorporating steam into the reduction-roasting process of spent lithium-ion batteries. *Waste Manage* **2021,** *134*, 100-109.

21.Zhou, F.; Qu, X.; Wu, Y.; Zhao, J.; Gao, S.; Wang, D.; Yin, H., Vacuum pyrolysis of pine sawdust to recover spent lithium Ion batteries: the synergistic effect of carbothermic reduction and pyrolysis gas reduction. *ACS Sustain. Chem. Eng.* **2022,** *10* (3), 1287-1297.

22.Chen, X.; Wang, Y.; Li, S.; Jiang, Y.; Cao, Y.; Ma, X., Selective recycling of valuable metals from waste LiCoO2 cathode material of spent lithium-ion batteries through low-temperature thermochemistry. *Chem. Eng. J.* **2022,** *434*, 134542.

23.Meng, Z.; Huang, W.; Gao, L.; Dai, J.; Lu, X.; Liu, J.; Huang, H.; Shih, K.; Tang, Y., Green and energy-saving recycling of LiCoO2 by synergetic pyrolysis with polyvinyl chloride plastics. *ACS Sustain. Chem. Eng.* **2022,** *10* (37), 12329-12341.

24.Jehanno, C.; Alty, J. W.; Roosen, M.; De Meester, S.; Dove, A. P.; Chen, E. Y.; Leibfarth, F. A.; Sardon, H., Critical advances and future opportunities in upcycling commodity polymers. *Nature* **2022,** *603* (7903), 803-814.

25.Zhu, Y.; Romain, C.; Williams, C. K., Sustainable polymers from renewable resources. *Nature* **2016,** *540* (7633), 354-362.

26.Chen, G.; Tu, X.; Homm, G.; Weidenkaff, A., Plasma pyrolysis for a sustainable hydrogen economy. *Nat. Rev. Mater.* **2022,** *7* (5), 333-334.

27.Xu, Z.; Pan, F.; Sun, M.; Xu, J.; Munyaneza, N. E.; Croft, Z. L.; Cai, G. G.; Liu, G., Cascade degradation and upcycling of polystyrene waste to high-value chemicals. *Proc Natl Acad Sci U S A* **2022,** *119* (34), e2203346119.

28.Liu, Q.; Liu, S.; Lv, Y.; Hu, P.; Huang, Y.; Kong, M.; Li, G., Atomic-scale insight into the pyrolysis of polycarbonate by ReaxFF-based reactive molecular dynamics simulation. *Fuel* **2021,** *287*, 119484.

29.Demirbas, A., Pyrolysis of municipal plastic wastes for recovery of gasoline-range hydrocarbons. *J. Anal. Appl. Pyrolysis* **2004,** *72* (1), 97-102.

30.Zhou, H.; Ren, Y.; Li, Z.; Xu, M.; Wang, Y.; Ge, R.; Kong, X.; Zheng, L.; Duan, H., Electrocatalytic upcycling of polyethylene terephthalate to commodity chemicals and H2 fuel. *Nat. Commun.* **2021,** *12* (1), 4679.

31.Dai, Q., Spangenberger, Jeffrey, Ahmed, Shabbir, Gaines, Linda, Kelly, Jarod C., and Wang, Michael, EverBatt: A closed-loop battery recycling cost and environmental impacts model. *United States: N. p* **2019**.

32.Dong, F.; Han, W.; Han, W.; Tang, Z., Assembling core-shell SiO2@NiaCobOx nanotube decorated by hierarchical NiCo-Phyllisilicate ultrathin nanosheets for highly efficient catalytic combustion of VOCs. *Appl. Catal. , B.* **2022,** *315*, 121524.

33.Jiang, Y.; Xu, R.; Zeng, C.; Wang, K.; Han, L.; Zhang, X., Scalable decomposition-catalysis of disposable COVID-19 face mask over self-assembly metal-doping carbocatalysts for tunable value-added products. *Appl. Catal. , B.* **2022,** *317*, 121735.

34.Tian, W.-W.; Ren, J.-T.; Yuan, Z.-Y., In-situ cobalt-nickel alloy catalyzed nitrogen-doped carbon nanotube arrays as superior freestanding air electrodes for flexible zinc-air and aluminum-air batteries. *Appl. Catal. , B.* **2022,** *317*, 121764.

35.Yao, D.; Yang, H.; Hu, Q.; Chen, Y.; Chen, H.; Williams, P. T., Carbon nanotubes from post-consumer waste plastics: Investigations into catalyst metal and support material characteristics. *Appl. Catal. , B.* **2021,** *280*, 119413.

36.Zhu, Y.; Miao, J.; Long, M.; Wu, C., Feasibilities of producing high-value carbon nanotubes from waste plastics by spray pyrolysis. *J. Anal. Appl. Pyrolysis* **2022,** *166*, 105613.

37.Li, J.; Lai, Y.; Zhu, X.; Liao, Q.; Xia, A.; Huang, Y.; Zhu, X., Pyrolysis kinetics and reaction mechanism of the electrode materials during the spent LiCoO(2) batteries recovery process. *J. Hazard Mater* **2020,** *398*, 122955.

38.Gim, J.; Zhang, Y.; Gao, H.; Xu, G.-L.; Guo, F.; Ren, Y.; Amine, K.; Chen, Z., Probing solid-state reaction through microstrain: A case study on synthesis of LiCoO2. *J. Power Sources* **2020,** *469*, 228422.

39.Windisch-Kern, S.; Holzer, A.; Ponak, C.; Hochsteiner, T.; Raupenstrauch, H., Thermal analysis of lithium ion battery cathode materials for the development of a novel pyrometallurgical recycling approach. *Carbon Resour. Convers.* **2021,** *4*, 184-189.

40.Emelina, A. L.; Bykov, M. A.; Kovba, M. L.; Senyavin, B. M.; Golubina, E. V., Thermochemical properties of lithium cobaltate. *Russ. J. Phys. Chem. A* **2011,** *85* (3), 357-363.

41.Hou, J.; Feng, X.; Wang, L.; Liu, X.; Ohma, A.; Lu, L.; Ren, D.; Huang, W.; Li, Y.; Yi, M.; Wang, Y.; Ren, J.; Meng, Z.; Chu, Z.; Xu, G.-L.; Amine, K.; He, X.; Wang, H.; Nitta, Y.; Ouyang, M., Unlocking the self-supported thermal runaway of high-energy lithium-ion batteries. *Energy Storage Materials* **2021,** *39*, 395-402.

42.Li, Y.; Liu, X.; Wang, L.; Feng, X.; Ren, D.; Wu, Y.; Xu, G.; Lu, L.; Hou, J.; Zhang, W.; Wang, Y.; Xu, W.; Ren, Y.; Wang, Z.; Huang, J.; Meng, X.; Han, X.; Wang, H.; He, X.; Chen, Z.; Amine, K.; Ouyang, M., Thermal runaway mechanism of lithium-ion battery with LiNi0.8Mn0.1Co0.1O2 cathode materials. *Nano Energy* **2021,** *85*, 105878.

43.Dai, L.; Zhou, N.; Lv, Y.; Cheng, Y.; Wang, Y.; Liu, Y.; Cobb, K.; Chen, P.; Lei, H.; Ruan, R., Pyrolysis technology for plastic waste recycling: A state-of-the-art review. *Prog. Energy Combust. Sci.* **2022,** *93*, 101021.

44.Zhou, N.; Dai, L.; Lv, Y.; Li, H.; Deng, W.; Guo, F.; Chen, P.; Lei, H.; Ruan, R., Catalytic pyrolysis of plastic wastes in a continuous microwave assisted pyrolysis system for fuel production. *Chem. Eng. J.* **2021,** *418*, 129412.

45.N, S., Plastic waste management: A road map to achieve circular economy and recent innovations in pyrolysis. *Sci Total Environ* **2022,** *809*, 151160.

46.Yuan, Z.; Huang, Q.; Wang, Z.; Wang, H.; Luo, J.; Zhu, N.; Cao, X.; Lou, Z., Medium-Low temperature conditions induce the formation of environmentally persistent free radicals in microplastics with conjugated aromatic-ring structures during sewage sludge pyrolysis. *Environ. Sci. Technol.* **2022,** *56* (22), 16209-16220.

47.Jung, S.; Tsang, Y. F.; Kwon, D.; Choi, D.; Chen, W.-H.; Kim, Y.-H.; Moon, D. H.; Kwon, E. E., CO2-mediated thermal treatment of disposable plastic food containers. *Chem. Eng. J.* **2023,** *451*, 138603.

48.Kwon, D.; Jung, S.; Moon, D. H.; Tsang, Y. F.; Chen, W.-H.; Kwon, E. E., Strategic management of harmful chemicals produced from pyrolysis of plastic cup waste using CO2 as a reaction medium. *Chem. Eng. J.* **2022,** *437*, 135524.

49.Xue, Y.; Johnston, P.; Bai, X., Effect of catalyst contact mode and gas atmosphere during catalytic pyrolysis of waste plastics. *Energy Convers. Manage.* **2017,** *142*, 441-451.

50.Liu, R.; Zhao, S.; Zhang, B.; Li, G.; Fu, X.; Yan, P.; Shao, Z., Biodegradation of polystyrene (PS) by marine bacteria in mangrove ecosystem. *J. Hazard Mater* **2023,** *442*, 130056.

51.Li, M.; Zhang, B.; Qu, X.; Cai, M.; Liu, D.; Zhou, F.; Xie, H.; Gao, S.; Yin, H., A SiCl4-assisted roasting approach for recovering apent LiCoO2 cathode. *ACS Sustain. Chem. Eng.* **2022,** *10* (26), 8305-8313.